Polskie Towarzystwo Materiałów Kompozytowych
Polish Society of Composite Materials

26: 2 (2026) 76–87

COMPOSITES THEORY AND PRACTICE

ISSN (online): 2299-128X

Kalyanamanohar Veeramallu[1]*, Tarun Kumar Kotteda[2], Vimala Raghavan[3], Prabhakar Undre[4], S. Shailajha[5], Mishikari Nizamoddin[1]

[1] *Department of Mechanical Engineering, University College of Engineering Kakinada (A), JNTU Kakinada, Andhra Pradesh, 533003, India*
[2] *Department of Mechanical Engineering, Sagi Rama Krishnam Raju Engineering College, Bhimavaram-534204, Andhra Pradesh, India*
[3] *Centre for Nanotechnology Research, Vellore Institute of Technology, Vellore-632014, India*
[4] *Advanced Functional Materials Lab, Department of Physics, Dr Babasaheb Ambedkar Marathwada University, Aurangabad, Maharashtra-431004, India*
[5] *Department of Physics, Manonmaniam Sundaranar University, Tirunelveli – 627012, Tamil Nadu, India*
* *Correspondence*: kalyanamanohar@jntucek.ac.in

Received (Otrzymano) 7.01.2026
Published on-line (Opublikowano) 30.06.2026

DEVELOPMENT AND CHARACTERIZATION OF MG-NHAP-GNP HYBRID COMPOSITES FOR BIOMEDICAL APPLICATIONS

https://doi.org/10.62753/ctp.2026.04.2.2

Traditional metallic materials, including titanium and stainless steel, offer excellent biocompatibility and function widely as orthopaedic implants for fracture fixation. However, their non-biodegradable nature creates a major limitation in long-term biomedical use. Magnesium emerges as a promising alternative for implant applications due to its inherent biodegradability. In the present investigation, nano-hydroxyapatite (nHAP) at 10 wt% together with graphene nanoplatelets (GNP) at 0.1, 0.2, and 0.3 wt% underwent incorporation into magnesium by means of pressureless sintering, then the mechanical and microstructural behaviour of the resulting material was investigated. The phase quality and microstructural features were examined using X-ray diffraction (XRD) and scanning electron microscopy (SEM). The mechanical performance of the Mg hybrid composites was assessed utilising a Vickers micro-hardness tester, a universal tensile testing machine, and a pin-on-disc tribometer. SEM observations revealed uniform dispersion of nHAP across the grains, while GNP predominantly occupied the grain boundaries. A notable increase in tensile strength and hardness emerged with the GNP addition, yielding a hardness value of 66.74 HV1, primarily due to grain refinement. Owing to the self-lubricating nature of GNP, the composite with 0.2 wt% GNP exhibited a reduced wear rate of 0.000793 mm^3/Nm in comparison with monolithic Mg. Furthermore, enhanced hardness contributed to lower wear, aligning with Archard's law.

Keywords: magnesium, nano hydroxyapatite, graphene nanoplatelets, powder metallurgy, sintering

INTRODUCTION

Magnesium and its alloys have a special place among lightweight structural metals and have a perfectly good opportunity to become an important part of the future biomedical and automotive industry with the massive weight savings and an equal increase in functional efficiency being of paramount significance [1, 2]. The growing demand for bio-implants, including artificial organs, hard tissue replacements, and bone fixation devices in recent years has resulted in the creation of many innovative biomaterials [3]. Popular types of materials for implants such as stainless steel, cobalt-chromium alloys, and titanium alloys are very strong, although not biodegradable [4]. Their elastic modulus, strength and density are very different to natural bone and as such, local stress levels concentrate on the implant itself, usually known as the stress-shielding effect [5]. This effect is usually accompanied by intense pain, a loss of osteogenesis stability, and, finally, a limitation

of bone regeneration [6]. Traditional bio-implants as bone fixatives are usually removed by secondary surgery after tissue growth, which adds another medical expense as well as significant psychological discharge to the patient [7, 8]. Taking into account the restrictions related to the use of traditional hard-metal implants, magnesium alloys and composites appeared as potential materials to be used as inserts and bone-fixation devices because of their high levels of biodegradability, high biocompatibility, and elastic modulus that is similar to that of bone [9]. However, rapid degradation after implantation, along with limited mechanical and corrosion performance, restricts the suitability of Mg for load-bearing biomedical applications [10]. To address these problems, one way of improving the biocompatibility and mechanical characteristics of Mg would be to alloy it with appropriate reinforcement materials.

Conversely, nano hydroxyapatite (nHAP) is a bio-ceramic material that is highly compatible with bone and dental enamel. Besides, nHAP has superior mechano-biological, antibacterial and corrosion control properties. Xiong et al. [11] developed nHAP-reinforced magnesium composites by means of microwave-assisted sintering, and 10 wt% nHAP-reinforced Mg composites exhibited significant improvement in the physical properties and mechanical behaviour compared to pure Mg. Guo et al. [12] reported on their success in the use of spark plasma sintering to form Mg-nHAP alloys. The impact of 10 wt% nHAP provided better mechanical strength and resistance to corrosion compared to other alloy systems. These authors concluded that the highest biocompatibility and mechanical performance were at 10 wt% nHAP. Singh et al. [13] successfully fabricated a porous Mg-Zn-Mn-HA alloy by mechanical alloying Mg, Mn, Zn, and HA powders, followed by consolidation using the microwave-assisted spark plasma sintering technique. The resulting alloy registered a maximum micro-hardness of 97 Hv, which was significantly higher compared to other values generally recorded for traditional Mg alloys. By combining nHAP with Mn and Zn, the grain structure was refined, and the bio-corrosion properties were enhanced.

Over the last few years, graphene nanoplatelets (GNP) have attracted extensive attention in terms of improving the mechanical response of metal matrices because of the numerous strengthening mechanisms; moreover, these nanoparticles are characterized by high biocompatibility [14, 15]. An addition of GNP to Mg matrix composites significantly enhances the mechanical properties, particularly Young's modulus, the tensile strength, yield strength, and fracture strain as a consequence of the effective load transfer and high specific surface area of GNP [16]. The incorporation of GNP in metal matrices promotes grain refinement and improves the interfacial characteristics with effective dispersion within the matrix. In addition, uniformly distributed GNP can hinder grain growth and contribute to enhanced composite properties [17, 18]. Rashad et al. [19] investigated the electrochemical corrosion behaviour of GNP reinforced AZ31 and AZ61 magnesium alloys in a 3.5 wt% NaCl solution by means of polarization studies. The results showed that the incorporation of GNP increased the corrosion current density and shifted the corrosion potential toward more negative values compared to the unreinforced alloys, mainly owing to the galvanic interactions between the conductive GNP and Mg matrix. The study further reported that non-uniform GNP distribution and localized galvanic coupling promoted pitting corrosion in the composites.

According to Brezina et al. [20], magnesium exhibits significant potential for biomedical applications on account of its favourable mechanical compatibility and non-toxic nature; nonetheless, its high chemical reactivity limits wider practical implementation. Their study demonstrated that powder metallurgy processing effectively enhanced the mechanical and electrochemical performance of pure Mg by means of cold compaction and hot pressing. The processed samples exhibited substantial improvement in strength (up to 250 MPa) and microhardness (65 HV, 0.025 kg load) compared with conventionally prepared Mg. Furthermore, the application of compressive stress in the range of 300–500 MPa was reported to positively influence both the mechanical integrity and corrosion-related behaviour of the material. Yan et al. [21] showed that magnesium alloys have a good potential to be biodegradable biomedical materials because they exhibit the following characteristics: good mechanical properties and high levels of biocompatibility. Shahin et al. [22] also reported that magnesium and magnesium alloys

have potentials to serve as biodegradable implants because of their strength and ability to degrade naturally in the body.

All the aforementioned works point to the possibility of using GNP as a potent reinforcement to prepare MMnCs with improved mechanical and corrosion resistant properties. The current research entails the production of bio-composites with Mg, 10 wt% nHAP and GNP additions of 0.1, 0.2 and 0.3 wt% by means of a pressureless sintering method. The obtained hybrid composites were examined using XRD and SEM, while the hardness and wear were tested to determine how the properties of the composites in terms of structure and mechanical properties function.

MATERIALS AND METHODS

Materials

The matrix material was commercially available pure magnesium powder (Neeraj Industries, India) with a particle size of 45 μm. The reinforcements were nano hydroxyapatite powder (All India Metal Corporation, India) with a particle size of 5–10 nm and graphene nanoplatelets (United Nanotech Pvt. Ltd, India) with a thickness of 3–5 nm. Table 1 presents a comparison of the mechanical properties of different implant materials and cortical bone to highlight the differences in their performance.

TABLE 1. **Mechanical properties of implant materials and cortical bone [23]**

Material/tissue	Density (g/cm^3)	Elastic modulus (MPa)	Ultimate tensile strength (MPa)	Yield stress (MPa)
Cortical bone	1.8-2	5-23	35-283	104.9-114.3
Ti-6Al-4V	4.43	114	830-1025	760-880
SS316L	8	190	450-650	200-300
Magnesium	1.78	45	160-250	90-160

Experimental part

Initially, Mg powder and 10 wt% nHAP were blended according to the compositions listed in Table 2, while the GNP reinforcement content was varied from 0 to 0.3 wt% at intervals of 0.1 wt%, with a corresponding reduction in the Mg content to maintain the overall composition at 100 wt%. The constituent powders were separately dispersed in ethanol and homogenized utilising a magnetic stirrer to obtain a uniform suspension. Subsequently, the mixture was heated on a hot plate for 1 h to evaporate the ethanol and obtain a dried ultrafine powder mixture, which was then subjected to high-energy planetary ball milling. Ball milling was done at a ratio of 10:1 and 200 rpm with ethanol as the milling medium. The mixture was milled for 2 hours and afterwards the slurry was dried on a hot plate to obtain an evenly mixed ultra-fine powder. Zinc stearate was put along the die walls to form a lubricant and also to ensure that the release of the punches was easy during compaction. The ultra-fine mixture was put between two rigid punches and then compacted by means of a uniaxial hydraulic press at a pressure of less than 400 MPa. Then green rectangular coupons of 65 x 15 x 5 mm were put into a tubular vacuum furnace and pressureless sintered at 550ºC with a holding period of 120 min at a vacuum level of 0.001 mbar. The coupons subsequently underwent furnace cooling to room temperature. Figure 1 depicts the experimental flow followed to develop the composite samples. The same sequence of fabrication aided the manufacture of all the hybrid composites as presented in Table 2.

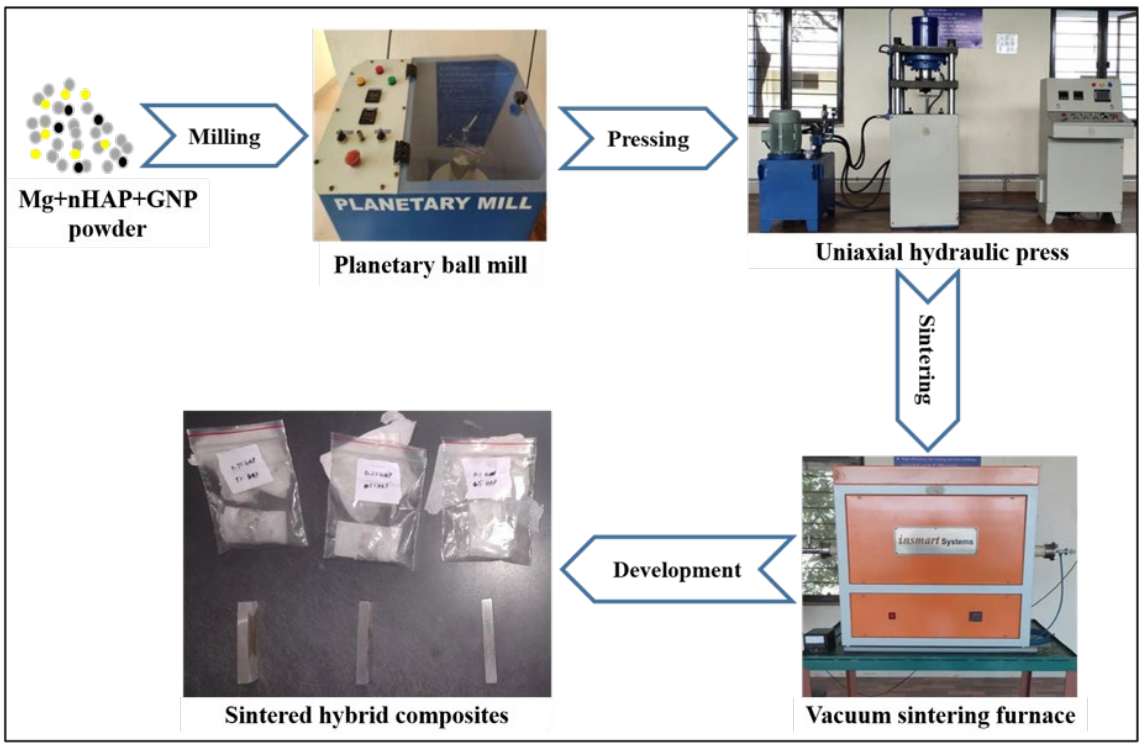

Fig. 1. Experimental flow for sample fabrication

TABLE 1. **Nomenclature of developed composite samples**

Sample	Nomenclature
M0	90 wt% Mg + 10 wt% nHAP
M1	89.9 wt% Mg + 10 wt% nHAP + 0.1 wt% GNP
M2	89.8 wt% Mg + 10 wt% nHAP + 0.2 wt% GNP
M3	89.7 wt% Mg + 10 wt% nHAP + 0.3 wt% GNP

Density

The sintered density of each of the samples was measured using the Archimedes principle with distilled water as the medium of immersion. The density of each sample was measured three times to obtain the average sintered density, which was obtained by the standard Archimedes relation. Each composite formulation had a theoretical density based on the rule of mixtures, which gave a good reference point against which to compare the experimentally determined data.

$$Sintered\ density = \frac{Weight\ in\ air}{Weight\ in\ air - weight\ in\ water} \quad (1)$$

$$\text{Composite theoretical density } (\rho_{th}) = \left(\frac{Wf\ of\ Mg}{\rho\ \text{of Mg}} + \frac{Wf\ of\ HAP}{\rho\ of\ HAP} + \frac{Wf\ of\ GNP}{\rho\ of\ GNP}\right)^{-1} \quad (2)$$

$$\text{Relative density} = \frac{Sintered\ density}{Theoretical\ density}\ \text{X}\ 100\ \% \quad (3)$$

The theoretical density for Mg, nHAP and GNP had values of 1.8, 3.1 and 2.1 g/cm^3, respectively, drawn directly from supplier datasheet.

XRD and metallography

The surface preparation of specimens was performed utilising a double-disc polishing machine with 180, 600, 1000, 1500, 2000 and 4000 grade emery papers and water-mixed alumina was applied to a partial mirror finish. A full mirror surface was produced by subsequent treatment with diamond paste. The specimens were subsequently etched with a suspension of picric acid (3 ml), ethanol (50 ml), acetic acid (5 ml) and distilled water (20 ml). Microstructural analysis of the etched specimens was done by means of an optical microscope (BX53M, Olympus, Japan) and a scanning electron microscope (VEGA 3, SBH TESCAN Brno SRO). Phase analysis of the composites was successively carried out on an X-ray diffractometer (RIGAKU, SMART LAB SE, Japan) at 45 kV and 30 mA with Cu-K a radiation (λ = 0.15406 nm). XRD parameters of a 2θ range of 20º-80º and a scanning speed of 5º/min were applied.

Composite testing

Vickers hardness testing was performed using a Vickers microhardness tester (FMV-1, FSA Pvt. Ltd) with a load of 500 gf and the test was conducted at three different points on the specimen to obtain a mean value. The same procedure was repeated on all the prepared specimens. Prismatic specimens for wear testing were fabricated in accordance with ASTM 99 and were tested at ambient temperature employing a pin-on-disc device (DUCOM, USA). The wear test conditions were: 10 N load, counter body of EN 31 steel (62 HRC) and a sliding speed of 1 m/s to ensure similar evaluation. The wear rate of the specimens was calculated using the following equations [24].

$$\text{Wear rate } (W_r) = \frac{Change\ in\ volume\ (\Delta V)}{Load \times distance}\ \text{mm}^3/\text{Nm} \quad (4)$$

$$\text{Change in volume } (\Delta V) = \frac{Weight\ loss}{Density}\ \text{mm}^3 \quad (5)$$

RESULTS AND DISCUSSION

Phase analysis

The X-ray diffraction (XRD) patterns of the M0, M1 and M2 specimens were recorded in the 20°–80° range of analysis at a scanning rate of 5º/min as shown in Figure 2. The diffraction profiles show clear sharp reflections of magnesium and hydroxyapatite (HAP), which indicate the presence of both phases in the composite specimens [12, 25]. Expectedly, no GNP peak was observed in the XRD spectra of any of the hybrid composites, which is explained by the fact that the GNP concentration in the Mg matrix was low [26]. This same explanation was found in the results of Kalyanamanohar et al. [27], where the XRD results of graphene reflections were not detected in the analysis. There are also minor MgO reflections at 63º along with the prevailing Mg and HAP peaks [28]. These peaks are as a result of the oxidation of magnesium on the surface during processing and/or being exposed to atmospheric oxygen. Since it is very reactive, magnesium forms a thin layer of MgO, especially when exposed to higher temperatures that occur during the sintering process or when the composite is being produced. Similar findings can be observed in previous studies of Mg-HAP and Mg-based materials, in which trace MgO phases often formed during processing by reactions between magnesium and environmental oxygen as reported by Annur et al. [29]. Nevertheless, magnesium oxide is non-toxic and does not adversely affect the biocompatibility of the composite [30].

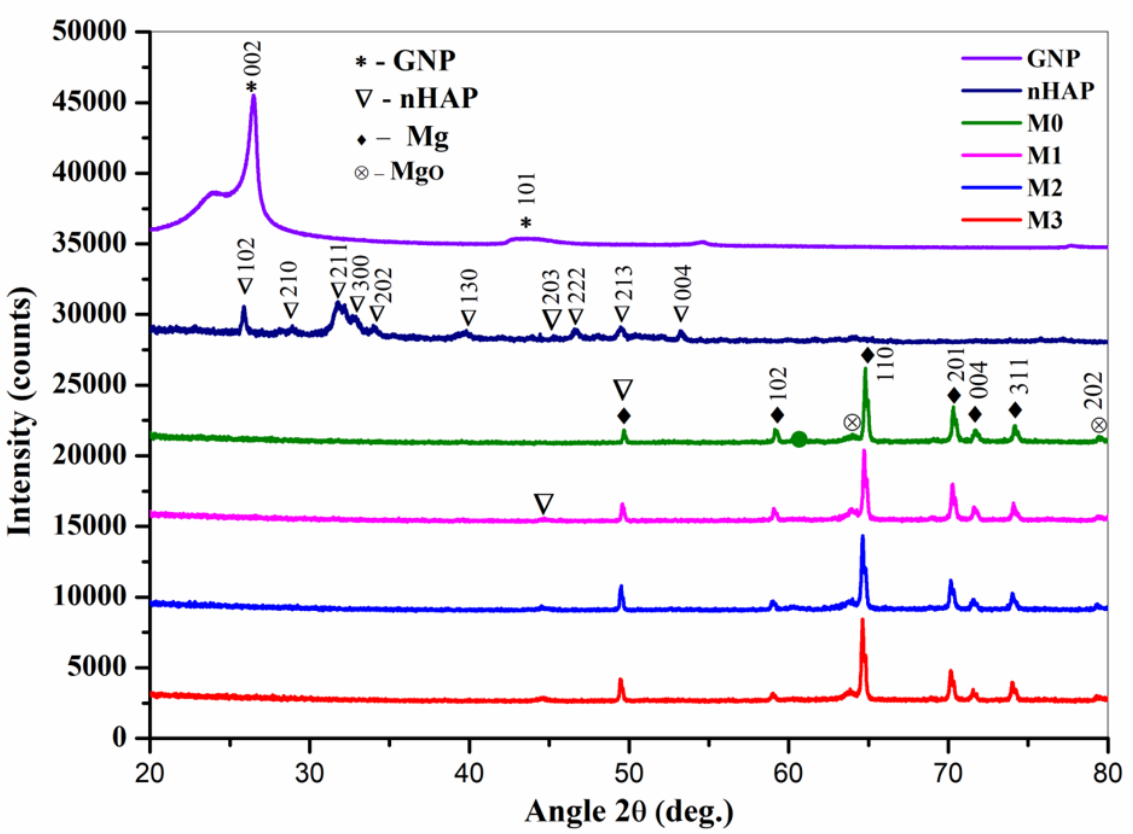

Fig. 2. X-Ray diffraction of composites

Densification

Table 3 shows the bulk densities, theoretical densities obtained by the rule of mixture and the relative density values of the composites. The pores of the M0 composite are relatively small in comparison with the other samples. The relative density grows slightly with an increase in GNP content in the Mg-nHAP composites, primarily because of the homogeneity in the positioning of nanoparticles between the grains of magnesium. The M2 composite has a greater relative density in comparison to M3, which has a more homogenous distribution of reinforcements. However, pores or porosity often become an inherent effect of composite metallurgy along powder metallurgy pathways. Interestingly, functional benefits to biomaterials are often provided by a controlled level of surface porosity, especially to bone-support implants. These pores serve as good microsites of cell adhesion and subsequent growth, thus supporting tissue regeneration, enhancing the repair of broken bone, and the process of osseointegration [31].

TABLE 2. **Density, hardness and wear rate of composite samples**

Sample name	Theoretical density (gm/cm^3)	Bulk density (gm/cm^3)	Relative density (%)	Hardness (Hv)	Grain size (μm)	Wear rate (mm^3/Nm)
M0	1.8789	1.828	97.3	49.62±0.26	15.54±0.31	0.00106
M1	1.8793	1.825	97.1	55.25±0.30	12.53±0.22	0.000985
M2	1.8811	1.845	98.1	66.74±0.36	8.98±0.17	0.000793
M3	1.8830	1.860	98.7	58.69±0.29	10.48±0.16	0.000875

Composite hardness

The Vickers microhardness test of M0, M1, M2 and M3 was performed using 50 g on all the specimens at various positions to obtain an average hardness value. The respective findings are presented in Figure 3. The hardness of the M2 composite (66.74 HV1) shows a moderate increase with the addition of GNP content in it relative to M0, whereas a significant decline is observed in the M3 composite (58.69 HV1), which may be attributed to the agglomeration of GNPs at higher reinforcement contents, leading to increased porosity and reduced interfacial bonding [32]. The rise in the hardness is mostly due to the additions of hard ceramic HAP particles and GNP to the soft magnesium matrix [27, 33]. This enhancement is created by even distribution of nHAP and GNP across the grain boundaries, which facilitates efficient indentation resistance. The additional grain refinement in the M2 composite further inhibits the movement of dislocations during loading, hence increasing the resistance of deformation. Furthermore, the growth in hardness of M2 is comparable to the projections made by the Hall Petch relation [27]. These observations highly correspond with the conclusions made in previous studies by other researchers [34, 35].

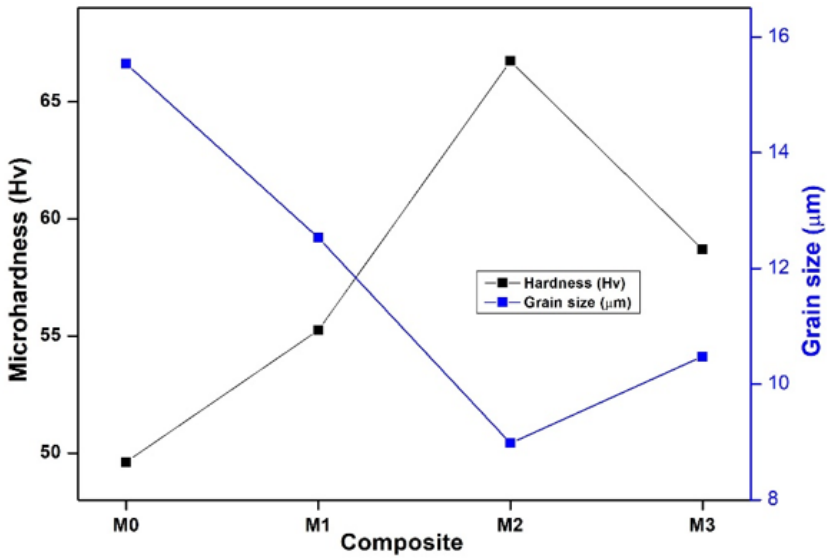

Fig. 3. Variation in microhardness and grain size of composites

Average grain size

Grain refinement in the composites was assessed using the linear intercept technique with ImageJ software. The optical micrograph of the M0 composite shows a coarse and anisotropic grain morphology with a mean grain size of 15.54 μm (Figure 4a). This anisotropy often arises during the uniaxial hydraulic pressing stage of the powder metallurgy process, where the application of pressure (400 MPa) can lead to deformation of the magnesium powder particles along the pressing direction, resulting in elongated and anisotropic grains after sintering [36]. During subsequent pressureless sintering at 550ºC, the addition of GNP to the M1, M2 and M3 composites (0.1-0.3 wt%) accumulates along the grain boundaries and acts as an anchoring mechanism, which results in significant grain refinement with grain sizes of 12.53, 8.98 and 10.48 μm respectively (Figure 4b-d). The small initial sizes of nHAP (10-20 nm) and GNP (3-5 nm) help in reducing the grain size after sintering. Although their exact sizes may change resulting from possible agglomeration during processing, their fine size helps them disperse well in the matrix and restrict grain growth. This is supported by the noticeable reduction in grain size observed in the composites (Figure 4b-d), confirming their role in grain refinement. On the other hand, the M3 composite shows partial agglomeration owing to the higher percentage of GNP that slightly reduced the grain refinement effect.

Wear rate

Figure 5 presents the difference in the wear rates of the sintered M0, M1, M2, and M3 specimens at a constant load of 10 N. The wear rates of the fabricated specimens are arranged in decreasing order; M0 > M1 > M2 and the respective microhardness of the specimens are 49.62 HV1 > 55.25 HV1 > 66.74 HV1. Archard's law [37] suggests that the wear rates of materials with higher hardness are generally lower and the wear at increased applied loads is higher. In metallic systems, wear resistance is often a factor that is directly proportional to hardness levels [38, 39]. The decreased wear rate of the M2 composite is the result of the self-lubricating nature of GNP, which is explained by its graphite architecture. Besides this, grain refinement in the Mg matrix leads to enhanced wear resistance as the scattered GNP introduce obstacles to the motion of dislocation under applied loads [40].

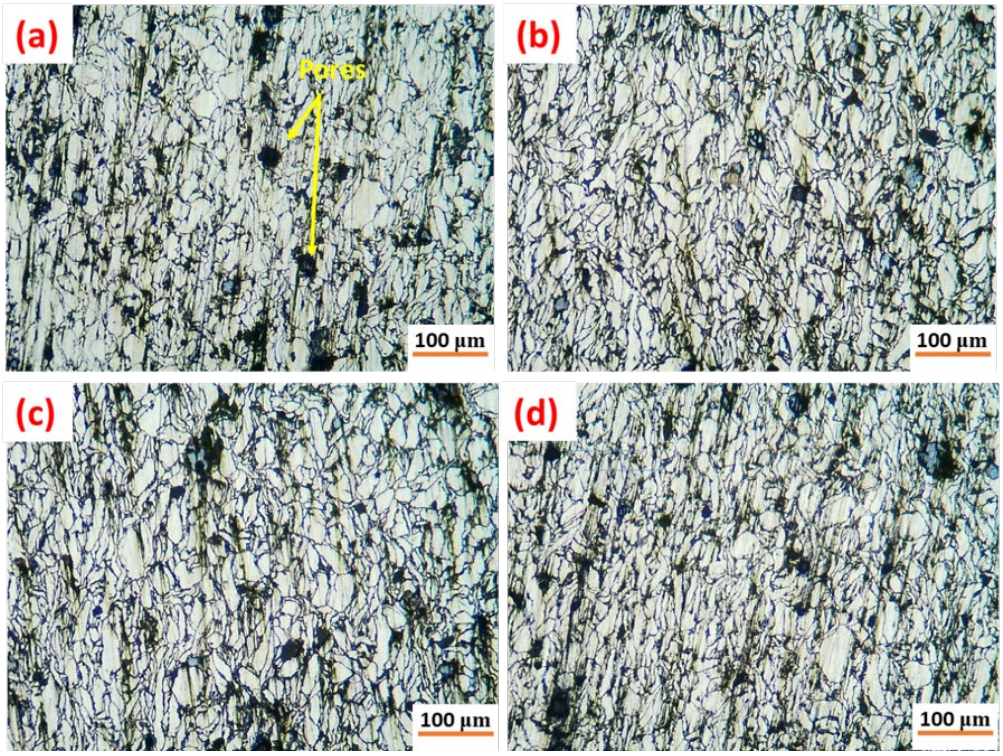

Fig. 4. Optical micrographs of (a) M0 (b) M1 (c) M2, and (d) M3 composites

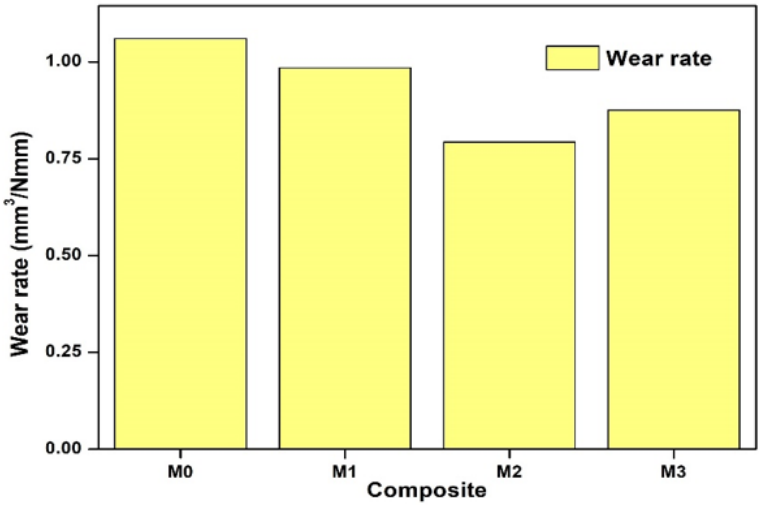

Fig. 5. Variation in wear rate of composite specimens

Microstructural analysis

The M0 composite specimen (Figure 6a) exhibited a dense morphology and non-equiaxed grain structure. The grain boundaries are clear on the surface with small spherical pores. The identification of GNP (dark regions) and nHAP (bright precipitates) in Figure 6(b) and (c) is based on the well-established principle of atomic number (Z) contrast and is consistent with morphological descriptions reported in the literature [41, 42]. Nevertheless, further compositional analysis is required for confirmation. Hydroxyapatite particles act as barriers during the solidification process, creating a Zener pinning effect that restricts grain growth. GNP also help reduce the grain size because they have high thermal conductivity and a lower coefficient of thermal expansion than magnesium. In addition, they are well dispersed within the magnesium matrix and are located along the grain boundaries, which lead to further grain refinement. These results are in close agreement with earlier studies [43-49]. Conversely, the M3 composite (Figure 6c) exhibited localized GNP agglomeration in a number of sites at the boundaries, which also led to lower hardness and lower wear resistance.

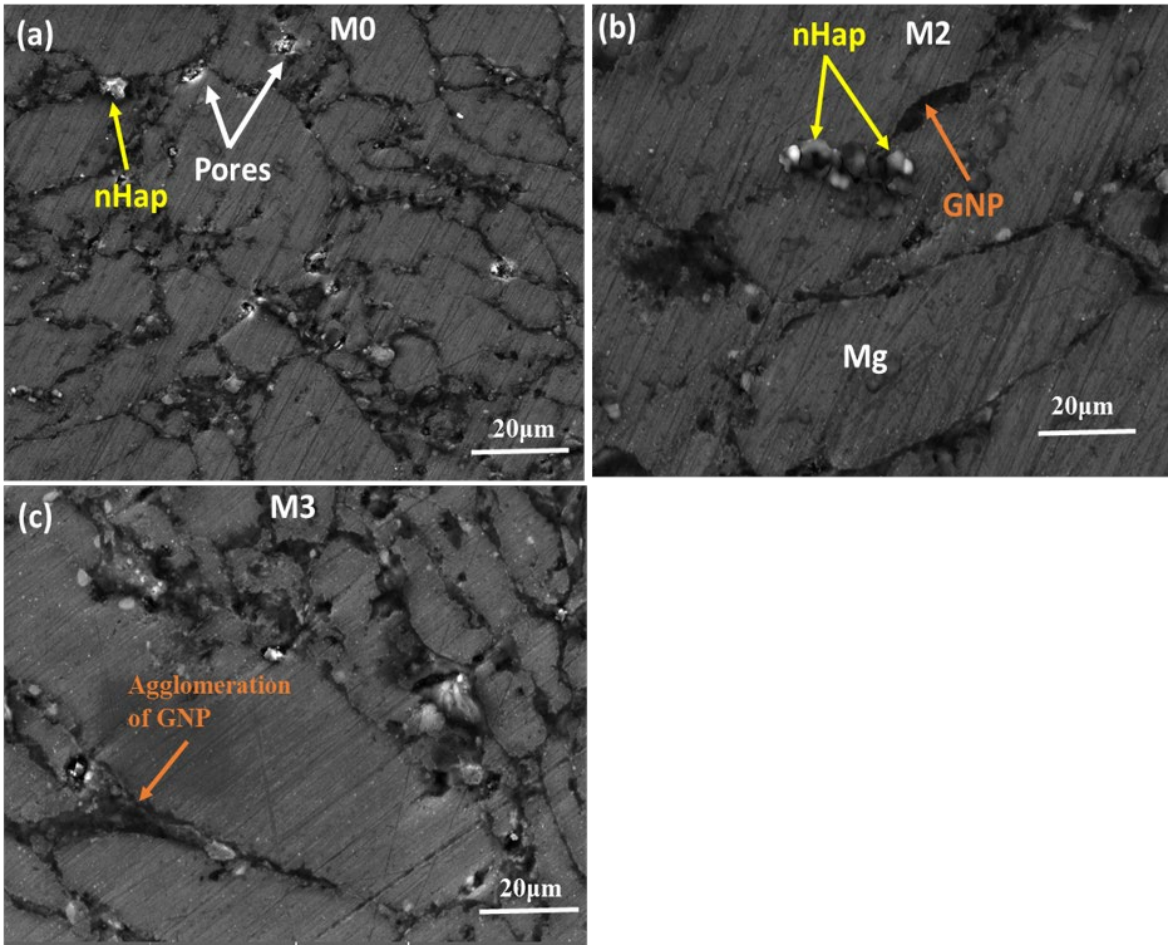

Fig. 6. Morphology of (a) M0, (b) M2 and (c) M3 composites

CONCLUSIONS

In the current work, magnesium hybrid composites reinforced with 10 wt% nano hydroxyapatite graphene nanoplatelets in the quantity of 0.1-0.3 wt% with regular intervals of 0.1 wt% were fabricated. The major findings are as follows:

- SEM revealed uniform distribution of the nHAP particles in magnesium with GNP alignment at the grain boundaries.
- The uniform distribution enhanced the effective transfer of loads and significant strengthening of the grain boundaries, which eventually

lead to increased hardness values. A maximum hardness of 66.74 HV1 was exhibited by the M2 composite, reflecting nearly a 14% enhancement over the magnesium composite without nHAP.

- The reinforcements offered by the nHAP and GNP synergies provided significant wear resistance enhancement caused by the ceramic properties of nHAP and self-lubricating behaviour of GNP. Nonetheless, the wear rate decreased with increasing GNP content because of the formation of a lubricating tribolayer at the contact interface, which reduced friction and minimized material removal during sliding.

The results of this study verify the beneficial microstructure and mechanical performance of Mg/nHAP/GNP hybrid composites. In turn, in vivo investigations are necessary on a large scale to evaluate both the biodegradability as well as biocompatibility, and the results are intended to be published in the future.

Data availability statement

The raw/processed data required to reproduce these findings cannot be shared at this time as the data also forms part of ongoing study.

Declaration of competing interest

The authors declare that they have no known competing financial interests or personal relationships that could have appeared to influence the work reported in this paper.

Acknowledgment

This research work was supported by the Anusandhan National Research Foundation (ANRF) under the Partnerships for Accelerated Innovation and Research (PAIR) project, Government of India, sanction order ANRF/PAIR/2025/000011/ PAIR-B.

REFERENCES

[1] Zhou T., Yang M., Zhou Z., Hu J., Chen Z., Microstructure and mechanical properties of rapidly solidified/powder metallurgy Mg–6Zn and Mg–6Zn–5Ca at room and elevated temperatures, J. Alloys Compd., 2013, 560, 161–166, DOI: 10.1016/j.jallcom.2013.01.066.

[2] Stulikova I., Smola B., Vlach M., Kudrnova H., Piesova J., Influence of powder metallurgy route on precipitation processes in Mg–Tb–Nd alloy, Mater. Charact., 2016, 112, 149–154, DOI: 10.1016/j.matchar.2015.12.020.

[3] Prakash C., Kansal H.K., Pabla B.S., Puri S., Aggarwal A., Electric discharge machining-a potential choice for surface modification of metallic implants for orthopedic applications: a review, Proc. Inst. Mech. Eng. Part B: J. Eng. Manuf., 2016, 230(2), 331–353, DOI: 10.1177/0954405415579113.

[4] Prakash C., Kansal H.K., Pabla B.S., Puri S., Processing and characterization of novel biomimetic nanoporous bioceramic surface on β-Ti implant by powder mixed electric discharge machining, J. Mater. Eng. Perform., 2015, 24(9), 3622–3633, DOI: 10.1007/s11665-015-1619-6.

[5] Al-Tamimi A.A., Peach C., Fernandes P.R., Cseke A., Bartolo P.J., Topology optimization to reduce the stress shielding effect for orthopedic applications, Procedia CIRP, 2017, 65, 202–206, DOI: 10.1016/j.procir.2017.04.032.

[6] Liu L., Koo Y., Collins B., Xu Z., Sankar J., Yun Y., Biodegradability and platelets adhesion assessment of magnesium-based alloys using a microfluidic system, PLoS One, 2017, 12(8), e0182914, DOI: 10.1371/journal.pone.0182914.

[7] Agarwal S., Curtin J., Duffy B., Jaiswal S., Biodegradable magnesium alloys for orthopaedic applications: a review on corrosion, biocompatibility and surface modifications, Mater. Sci. Eng. C, 2016, 68, 948–963, DOI: 10.1016/j.msec.2016.06.020.

[8] Brooks E.K., Ehrensberger M.T., Bio-corrosion of magnesium alloys for orthopaedic applications, J. Funct. Biomater., 2017, 8(3), 38, DOI: 10.3390/jfb8030038.

[9] Kaushik N., Sri Chaitanya C., Rao R.N., Abrasive grit size effect on wear depth of stir cast hybrid Al–Mg–Si composites at high stress condition, Proc. Inst. Mech. Eng. Part J: J. Eng. Tribol., 2018, 232(6), 672–684, DOI: 10.1177/1350650117726182.

[10] Cheng W., Bai Y., Wang L., Wang H., Bian L., Yu H., Strengthening effect of extruded Mg–8Sn–2Zn–2Al alloy: influence of micro and nano-size Mg_2Sn precipitates, Materials, 2017, 10(7), 822, DOI: 10.3390/ma10070822.

[11] Guo P., Cui Z., Yang L., Cheng L., Wang W., Xu B., Preparation of Mg/nano-HA composites by spark plasma sintering method and evaluation of different milling time effects on their microhardness, corrosion resistance, and biocompatibility, Adv. Eng. Mater., 2017, 19(1), 1600294, DOI: 10.1002/adem.201600294.

[12] Xiong G., Nie Y., Ji D., Li J., Li C., Li W., Wan Y., Characterization of biomedical hydroxyapatite/magnesium composites prepared by powder metallurgy assisted with microwave sintering, *Curr. Appl. Phys.*, 2016, 16(8), 830–836, DOI: 10.1016/j.cap.2016.05.004.

[13] Singh B.P., Singh R., Mehta J.S., Prakash C., Fabrication of biodegradable low elastic porous Mg–Zn–Mn–HA alloy by spark plasma sintering for orthopaedic applications, IOP Conf. Ser.: Mater. Sci. Eng., 2017, August, 225(1), 012050, DOI: 10.1088/1757-899X/225/1/012050.

[14] Kotteda T.K., Kumar M., Kumar P., Experimental insights and micrographical investigation on graphene nanoplatelet–reinforced aluminum cast composites, Int. J. Adv. Manuf. Technol., 2024, 131(5), 2707–2718, DOI: 10.1007/s00170-023-12270-8.

[15] Kotteda T.K., Kumar M., Kumar P., Gupta A., Kalidindi S.R.R., Mechanical and metallurgical behaviour of aluminum/graphene nanocomposites in fuselage applications, Cogent Eng., 2024, 11(1), 2324030, DOI: 10.1080/23311916.2024.2324030.

[16] Rashad M., Pan F., Hu H., Asif M., Hussain S., She J., Enhanced tensile properties of magnesium composites reinforced with graphene nanoplatelets, Mater. Sci. Eng. A, 2015, 630, 36-44, DOI: 10.1016/j.msea.2015.02.002.

[17] Saboori A., Moheimani S.K., Pavese M., Badini C., Fino P., New nanocomposite materials with improved mechanical strength and tailored coefficient of thermal expansion for electro-packaging applications, Metals, 2017, 7(12), 536, DOI: 10.3390/met7120536.

[18] Munir K.S., Qian M., Li Y., Oldfield D.T., Kingshott P., Zhu D.M., Wen C., Quantitative analyses of MWCNT–Ti powder mixtures using Raman spectroscopy: the influence of milling parameters on nanostructural evolution, Adv. Eng. Mater., 2015, 17(11), 1660–1669, DOI: 10.1002/adem.201500142.

[19] Rashad M., Pan F., Asif M., Chen X., Corrosion behavior of magnesium–graphene composites in sodium chloride solutions, J. Magnes. Alloys, 2017, 5, 271–276, DOI: 10.1016/j.jma.2017.06.003.

[20] Březina M., Minda J., Doležal P., Krystýnová M., Fintová S., Zapletal J., Ptáček P., Characterization of powder metallurgy processed pure magnesium materials for biomedical applications, Metals, 2017, 7(11), 461, DOI: 10.3390/met7110461.

[21] Yan Y., Cao H., Kang Y., Yu K., Xiao T., Luo J., Dai Y., Effects of Zn concentration and heat treatment on the microstructure, mechanical properties and corrosion behavior of as-extruded Mg–Zn alloys produced by powder metallurgy, J. Alloys Compd., 2017, 693, 1277–1289, DOI: 10.1016/j.jallcom.2016.10.017.

[22] Shahin M., Munir K., Wen C., Li Y., Magnesium-based composites reinforced with graphene nanoplatelets as biodegradable implant materials, J. Alloys Compd., 2020, 828, 154461, DOI: 10.1016/j.jallcom.2020.154461.

[23] Bommala V.K., Krishna M.G., Rao C.T., Magnesium matrix composites for biomedical applications: a review, J. Magnes. Alloys, 2019, 7(1), 72–79, DOI: 10.1016/j.jma.2018.11.001.

[24] Zhu X., Radovic-Moreno A.F., Wu J., Langer R., Shi J., Nanomedicine in the management of microbial infection-overview and perspectives, Nano Today, 2014, 9(4), 478–498, DOI: 10.1016/j.nantod.2014.06.003.

[25] Mohamad Rodzi S.N.H., Zuhailawati H., Dhindaw B.K., Mechanical and degradation behaviour of biodegradable magnesium–zinc/hydroxyapatite composite with different powder mixing techniques, J. Magnes. Alloys, 2019, 7, 566–576, DOI: 10.1016/j.jma.2019.11.003.

[26] Li F., Jiang X., Shao Z., Zhu D., Zhu M., Microstructure and mechanical properties of graphene-reinforced titanium matrix/nano-hydroxyapatite nanocomposites, Materials, 2018, 11(4), 608, DOI: 10.3390/ma11040608.

[27] Veeramallu K., Krishna A.G., Investigation of GNP effect on mechanical and morphological characteristics of liquid phase sintered SS316L nanocomposites processed via mechanical alloying and pressureless sintering, Compos. Theory Pract., 2024, 24, DOI: 10.62753/ctp.2024.03.2.2.

[28] ZabnAllah M. Alaizeri,Hisham A. Alhadlaq, Saad Aldawood, Maqusood Ahamed, Synthesis and Characterization of MgO-Fe_2O_3/γ-Al_2O_3 Nanocomposites: Enhanced Photocatalytic Efficiency and Selective Anticancer Properties, Catalysts 2024,14, 923.

[29] Annur D., Suhardi A., Amal M.I., Anwar M.S., Kartika I., Powder metallurgy preparation of Mg–Ca alloy for biodegradable implant application, J. Phys.: Conf. Ser., 2017, March, 817(1), 012062, DOI: 10.1088/1742-6596/817/1/012062.

[30] Ehsanollah Moradi, Mehdi Ebrahimian-Hosseinabadi, Mohammad Khodaei, Saeid Toghyani, Magnesium/Nano Hydroxyapatite porous biodegradable composite for biomedical applications, Mater. Res. Express 6 (2019) 075408.

[31] Vignesh P., Ramanathan S., Ashokkumar M., Sonar T., Ananthi V., Microstructure, mechanical, and electrochemical corrosion performance of Ti/HA (hydroxyapatite) particles reinforced Mg–3Zn squeeze casted composites, Int. J. Met., 2023, 18, 1348–1360, DOI: 10.1007/s40962-023-01114-6.

[32] Naik H.R., M. LH, Malik V., Patel G.C. M., Saxena K.K., Lakshmikanthan A., Effect of microstructure, mechanical and wear on Al-CNTs/graphene hybrid MMCs, Adv. Mater. Process. Technol., 2022, 8(Suppl. 2), 366–379, DOI: 10.1080/2374068X.2021.1927646.

[33] Thirugnanasambandam A., Mohankumar A., Botta R.P.R., Chong W.W.F., Thangamani G., Gupta M., Hydroxyapatite reinforced magnesium alloy composites using the ultrasonic-assisted rheo-squeeze casting technique: microstructural and mechanical performance evaluation for bone fixture applications, Crystals, 2024, 14(7), 667, DOI: 10.3390/cryst14070667.

[34] Saremi M., Kavusi N., Microstructure and mechanical properties of Mg-nano/micro hydroxyapatite composites made by powder metallurgy method, AIP Conf. Proc., 2017, 1896(1), 200011, DOI: 10.1063/1.5008248.

[35] Arora G.S., Saxena K.K., Mohammed K.A., Prakash C., Dixit S., Manufacturing techniques for Mg-based metal matrix composite with different reinforcements, Crystals, 2022, 12(7), 945, DOI: 10.3390/cryst12070945.

[36] Mariyappan Arul Kumar, M. Wronski, Irene J. Beyerlein, Controlling the Plastic Anisotropy of Magnesium Alloy by Tailoring the Grain Size and Yttrium Content, Crystals 2023, 13, 115.

[37] Vera-Cardenas E.E., Lewis R., Slatter T., Sliding wear study on the valve-seat insert contact, Open J. Appl. Sci., 2017, 7(2), DOI: 10.4236/ojapps.2017.72004.

[38] Yang J.B., Lin C.B., Wang T.C., Chu H.Y., The tribological characteristics of A356.2 Al alloy/Gr(p) composites, Wear, 2004, November, 257, 941–952, DOI: 10.1016/j.wear.2004.05.015.

[39] Ebrahimi M., Zarei-Hanzaki A., Abedi H.R., Azimi M., Mirjavadi S.S., Correlating the microstructure to mechanical properties and wear behavior of an accumulative back extruded Al–Mg_2Si in-situ composite, Tribol. Int., 2017, November, 115, 199–211, DOI: 10.1016/j.triboint.2017.05.034.

[40] Shahin M., Munir K., Wen C., Li Y., Nano-tribological behavior of graphene nanoplatelet-reinforced magnesium matrix nanocomposites, J. Magnes. Alloys, 2021, 9, 895-909, DOI: 10.1016/j.jma.2020.10.001

[41] Avila, J.D., Stenberg, K., Bose, S., Bandyopadhyay, A. (2021). Hydroxyapatite reinforced Ti6Al4V composites for load-bearing implants. *Acta biomaterialia*, *123*, 379–392.

[42] Segal, E., & Gedanken, A. (2015). Can r-graphene oxide replace the noble metals in SERS studies: the detection of acrylamide. *Environmental Chemistry*, *13*(1), 58–67.

[43] M. Kasaeian-Naeini, M. Sedighi, R. Hashemi, H. Delavar, Microstructure, mechanical properties and fracture toughness of ECAPed magnesium matrix composite reinforced with hydroxyapatite ceramic particulates for bioabsorbable implants, Ceram. Int. 49 (2023) 17074–17090.

[44] W. Zhai, X. Shi, M. Wang, Z. Xu, J. Yao, S. Song, Y. Wang, Grain refinement: a mechanism for graphene nanoplatelets to reduce friction and wear of Ni3Al matrix self-lubricating composites, Wear 310 (2014) 33–40.

[45] F. Chen, J. Ying, Y. Wang, S. Du, Z. Liu, Q. Huang, Effects of graphene content on the microstructure and properties of copper matrix composites, Carbon N Y 96 (2016) 836–842.

[46] S. Chinkanjanarot, J.M. Tomasi, J.A. King, G.M. Odegard, Thermal conductivity of graphene nanoplatelet/cycloaliphatic epoxy composites: Multiscale modeling, Carbon N Y 140 (2018) 653–663.

[47] K.S. Munir, M. Qian, Y. Li, D.T. Oldfield, P. Kingshott, D.M. Zhu, C. Wen, Quantitative analyses of MWCNT-Ti powder mixtures using raman spectroscopy: the influence of milling parameters on nanostructural evolution, Adv. Eng. Mater. 17 (2015) 1660–1669,

[48] K. Gusieva, C.H.J. Davies, J.R. Scully, N. Birbilis, Corrosion of magnesium alloys: the role of alloying, Int. Mater. Rev. 60 (2015) 169–194.

[49] M. Shahin, K. Munir, C. Wen, Y. Li, Magnesium-based composites reinforced with graphene nanoplatelets as biodegradable implant materials, J. Alloys Compd. 828 (2020).